2007-01-01

Slow Flow Between Concentric Cones

O. Hall
University of Exeter

C. P. Hills
Dublin Institute of Technology, chris.hills@dit.ie

A. D. Gilbert
University of Exeter

Recommended Citation

Hall, O., Hills, C.P. and Gilbert, A.D.: Slow Flow Between Concentric Cones. Quarterly Journal of Mechanics and Applied Mathematics,Vol, 60, Issue 1, 2007, pp.27-48.

SLOW FLOW BETWEEN CONCENTRIC CONES

by OSKAR HALL[†]

(*Mathematics Research Institute, School of Engineering, Computer Science and Mathematics, University of Exeter, Exeter* EX4 4QF)

CHRISTOPHER P. HILLS

(*School of Mathematical Sciences, Dublin Institute of Technology, Kevin Street, Dublin* 8, *Ireland*)

and ANDREW D. GILBERT[‡]

(*Mathematics Research Institute, School of Engineering, Computer Science and Mathematics, University of Exeter, Exeter* EX4 4QF)

[Received 25 July 2006. Revise 28 September 2006]

Summary

This paper considers the low-Reynolds-number flow of an incompressible fluid contained in the gap between two coaxial cones with coincident apices and bounded by a spherical lid. The two cones and the lid are allowed to rotate independently about their common axis, generating a swirling motion. The swirl induces a secondary, meridional circulation through inertial effects. For specific configurations complex eigenmodes representing an infinite sequence of eddies, analogous to those found in two-dimensional corner flows and some three-dimensional geometries, form a component of this secondary circulation. When the cones rotate these eigenmodes, arising from the geometry, compete with the forced modes to determine the flow near the apex.

This paper studies the relative dominance of these two effects and maps out regions of parameter space, with attention to how shear and overall rotation can destroy the infinite sequence of eddies that may be present when only the lid is rotated. A qualitative picture of the number of eddies visible in the meridional circulation is obtained as a function of the rotation rates of cones and lid, for various choices of angles. The results are discussed in the context of previous work, including their significance for applications to the mixing of viscous fluids in this geometry.

1. Introduction

Recirculatory regions, or eddies, are a well-known feature of many Stokes flows, and eddy structures have been found in a wide range of two- and three-dimensional geometries with corners. In many cases the eddies arise as eigenmodes of the geometry, which possess complex exponents of the distance to the corner, and hence the strength and size of the eddies decay exponentially as the corner is approached. The presence of such eddies is therefore determined not only by their relative dominance over other flow modes but also by the geometry. Moffatt (**1**) showed that for a

[†]⟨oskar.hall@gmail.com⟩
[‡]⟨a.d.gilbert@exeter.ac.uk⟩

Q. Jl Mech. Appl. Math, Vol. 60. No. 1
Advance Access publication 27 January 2007. doi:10.1093/qjmam/hbl024

two-dimensional corner the eddies can only exist if the angle of the corner is less than a cut-off angle, approximately 146° in (**2**), and that asymptotically they are the dominant flow feature as the apex is approached. At the cut-off angle, a pair of complex conjugate eigenvalues becomes real-valued: in our study we shall refer to this as a bifurcation as it represents a change in the streamline topology.

It is a common feature of low-Reynolds-number flows that, by exploiting linearity, the flow can be decomposed into two competing flow modes: one arising from the viscous driving and one whose structure is dictated purely by the geometry. Moffatt and Duffy (**2**) have discussed the relative dominance of flow modes for many two-dimensional similarity solutions. Hills (**3**) considered the three-dimensional eddies generated within a semi-infinite cylinder due to a rotating end-plate. The stream function can be decomposed into one component due to the viscous forcing and one part arising solely from the geometry which involves a complex exponent. The latter corresponds to a mode which decays more slowly than the forced component and hence dominates far away from the end-plate, giving an infinite sequence of eddies.

The conical geometry, in which a fluid is contained within a single cone of fixed half-angle β in spherical polar coordinates (r, ϑ, φ), has been studied by, amongst others, (**4** to **7**). In the case of axisymmetric disturbances, an infinite sequence of eddies can occur provided β is less than the cut-off value of $\beta_c \simeq 80{\cdot}9^\circ$ (**7**). Recently non-axisymmetric flows have been investigated by Malyuga (**5**) and Shankar (**6**). They both note that the dominant flow mode occurs for the azimuthal wave number $m = 1$ and that for this mode the critical angle equals $74{\cdot}45^\circ$.

The two-cone geometry is a natural extension of the Couette geometry but results in a base flow with three non-zero components of velocity, having many applications in fluid mixing and pumping (see for example (**8**, **9**)). The geometry of two truncated cones with the same angle α and parallel end walls has been considered both experimentally and numerically, predominantly in the context of Taylor–Couette flow; see for example (**10** to **12**). Rotation of the cones creates a circulating (meridional) flow due to the varying centrifugal forces and, at a critical Taylor number dependent upon several different factors, Taylor vortices appear (**12**).

An alternative two-cone geometry has, instead of parallel walls, cones with differing angles. The fluid now occupies the gap between coaxial cones with coincident apices having half-angles α and β with $\alpha < \beta$. Once again eddies can be present when the flow is driven by a far-field disturbance, for instance the rotation of a bounding lid. Hewitt (**13**) and Malhotra *et al.* (**14**) have considered this geometry and shown that the introduction of an inner cone, even at a very small angle α, has a dramatic effect on the critical angle β_c for eddies. For example when $\alpha = 0{\cdot}57^\circ$, $\beta_c \simeq 106^\circ$. Hewitt (**13**) and Malhotra *et al.* (**14**) have also described the eigenvalue distribution and bifurcations when β is further increased. Hynes (**15**) studied the flow between the cones when one of the cones is rotating, with particular attention to the cone-and-plane viscometer and the limiting case of rotating cylinders. He mapped out the region in parameter space where eddies will appear.

This paper provides a study of the dominant fluid behaviour for the slow flow between coaxial cones with coincident apices for different driving mechanisms. In particular we identify the appearance of eddies and bifurcations of the eigenvalues across a wide parameter range, allowing us to identify the features of most practical importance. The fluid is confined between the upper and lower cones $\vartheta = \alpha$, $\vartheta = \beta$ and a lid $r = r_0$, depicted in Fig. 1. Each of these three boundaries can rotate with an independent angular velocity, extending and generalizing the mechanisms considered previously. The primary flow is azimuthal but inertial forces induce a weaker meridional circulation. It is in this flow that Moffatt eddies can occur. We explicitly determine their appearance, arising

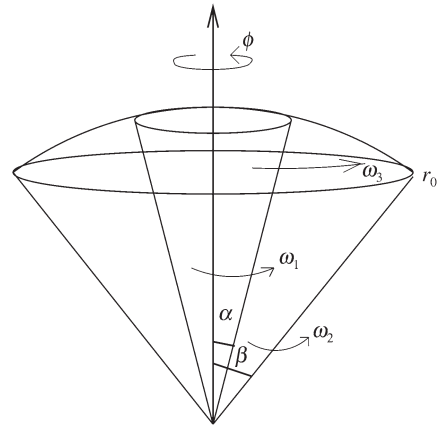

Fig. 1 The double cone geometry

from complex exponents of the geometrically controlled eigenfunctions, and their dominance over the directly forced component of the flow.

In section 2 we describe the geometry and parameters of the problem and set out the governing equations. The numerical method is described in section 3. In section 4 we discuss how driving can generate different flow components and highlight the competition between distinct effects: shearing by relative rotation of the upper and lower cones, overall rotation of upper and lower cones, and rotation of the lid. We illustrate our results by a number of examples for specific choices of cone angles. We explicitly map out the geometric exponents of the eigenmodes, including their bifurcations, as a function of cone angles α and β. An important issue for mixing is to determine which flow regimes possess a single eddy or very few eddies, reducing the number of separatrices which inhibit mixing. We map out the number of eddies the flow possesses for two choices of cone angles α and β. Throughout, comparison to previous results is made, in particular to the results of Hewitt (**13**) and Hynes (**15**), and in section 5 we discuss the implications of our results.

2. Governing equations

We consider an incompressible, linearly viscous fluid, of constant kinematic viscosity ν, contained between two conical surfaces with coincident apices and a lid, shown schematically in Fig. 1. In the spherical polar coordinate system (r, ϑ, φ), the conical surfaces are defined by $\vartheta = \alpha$ and $\vartheta = \beta$ respectively with $\alpha < \beta$, and independently rotate about their common axis with constant angular velocities ω_1 and ω_2. The fluid is enclosed by a spherical lid, $r = r_0$, which rotates with an angular speed ω_3.

We distinguish between three cases depending on how the motion is generated. If the cones are fixed ($\omega_1 = \omega_2 = 0$) and the motion is generated by the rotation of the outer spherical lid, we shall refer to this as case 1. Case 2 is when the spherical lid is held stationary ($\omega_3 = 0$) and one or both of the cones are rotating. Finally, case 3 refers to the general configuration when all three boundaries are in rotation.

The flow is assumed to be steady and axisymmetric. For convenience we non-dimensionalize lengths by r_0 and velocities by $r_0\omega_0$, where ω_0 is the maximum absolute value of ω_1, ω_2 and ω_3. We introduce a Reynolds number by $\mathrm{Re} = \omega_0 r_0^2/\nu$. In dimensionless units, we then introduce a stream function $\Psi(r,\vartheta)$ and a swirl function, $\boldsymbol{\Omega}(r,\vartheta)$, so that the velocity $(u_r, u_\vartheta, u_\varphi)$ is given by

$$u_r(r,\vartheta) = \frac{1}{r^2\sin\vartheta}\frac{\partial\Psi}{\partial\vartheta}, \quad u_\vartheta(r,\vartheta) = -\frac{1}{r\sin\vartheta}\frac{\partial\Psi}{\partial r}, \quad u_\varphi(r,\vartheta) = \frac{\boldsymbol{\Omega}}{r\sin\vartheta}.$$

The governing equations of the flow can be written as

$$\mathbb{D}^2\boldsymbol{\Omega} = \mathrm{Re}\left\{-\frac{1}{r^2\sin\vartheta}\frac{\partial(\Psi,\boldsymbol{\Omega})}{\partial(r,\vartheta)}\right\}, \tag{2.1a}$$

$$\mathbb{D}^4\Psi = \mathrm{Re}\left\{\frac{2\boldsymbol{\Omega}}{r^2\sin^2\vartheta}\left(\cos\vartheta\frac{\partial\boldsymbol{\Omega}}{\partial r} - \frac{\sin\vartheta}{r}\frac{\partial\boldsymbol{\Omega}}{\partial\vartheta}\right) - \frac{1}{r^2\sin\vartheta}\frac{\partial(\Psi,\mathbb{D}^2\Psi)}{\partial(r,\vartheta)} + \frac{2}{r^2\sin^2\vartheta}\left(\cos\vartheta\frac{\partial\Psi}{\partial r} - \frac{\sin\vartheta}{r}\frac{\partial\Psi}{\partial\vartheta}\right)\mathbb{D}^2\Psi\right\}, \tag{2.1b}$$

where $\mathbb{D}^2$ is the operator

$$\mathbb{D}^2 \equiv \frac{\partial^2}{\partial r^2} + \frac{\sin\vartheta}{r^2}\frac{\partial}{\partial\vartheta}\left(\frac{1}{\sin\vartheta}\frac{\partial}{\partial\vartheta}\right), \quad \text{and} \quad \frac{\partial(\Psi,\boldsymbol{\Omega})}{\partial(r,\vartheta)} = \frac{\partial\Psi}{\partial r}\frac{\partial\boldsymbol{\Omega}}{\partial\vartheta} - \frac{\partial\Psi}{\partial\vartheta}\frac{\partial\boldsymbol{\Omega}}{\partial r}.$$

The no-slip boundary conditions on the cones are

$$\boldsymbol{\Omega}(r,\alpha) = \omega_1 r^2\sin^2\alpha, \quad \boldsymbol{\Omega}(r,\beta) = \omega_2 r^2\sin^2\beta, \tag{2.2a}$$

$$\Psi(r,\alpha) = \Psi(r,\beta) = 0, \quad \frac{\partial\Psi}{\partial\vartheta}(r,\alpha) = \frac{\partial\Psi}{\partial\vartheta}(r,\beta) = 0, \tag{2.2b}$$

and on the lid

$$\boldsymbol{\Omega}(1,\vartheta) = \omega_3\sin^2\vartheta, \quad \Psi(1,\vartheta) = \frac{\partial\Psi}{\partial r}(1,\vartheta) = 0. \tag{2.3}$$

We are concerned with slow flows at low Reynolds numbers ($\mathrm{Re} \ll 1$) and write the stream function and swirl function as asymptotic expansions in Re. From (2.1) and the boundary conditions (2.2) and (2.3), at leading order the motion is purely swirling, which justifies the expansion,

$$\boldsymbol{\Omega}(r,\vartheta) = \boldsymbol{\Omega}_0(r,\vartheta) + \mathrm{Re}\,\boldsymbol{\Omega}_1(r,\vartheta) + \mathrm{Re}^2\,\boldsymbol{\Omega}_2(r,\vartheta) + \cdots,$$
$$\Psi(r,\vartheta) = \mathrm{Re}\,\Psi_1(r,\vartheta) + \mathrm{Re}^2\,\Psi_2(r,\vartheta) + \cdots.$$

Inertia induces a secondary meridional recirculation arising at $\mathcal{O}(\mathrm{Re})$, given by Ψ_1. It is possible to write $\boldsymbol{\Omega}_0$ and Ψ_1 as sums of forced modes and eigenmodes, and seek similarity solutions of the second kind (see (**16**)) for each,

$$\boldsymbol{\Omega}_0(r,\vartheta) = \boldsymbol{\Omega}_0^{\mathrm{p}} + \boldsymbol{\Omega}_0^{\mathrm{h}} = a_0 r^{\lambda_0} f_0(\vartheta) + \sum_{i=1}^{\infty} a_i r^{\bar{\lambda}_i}\bar{f}_i(\vartheta), \tag{2.4a}$$

$$\Psi_1(r,\vartheta) = \Psi_1^{\mathrm{p}} + \Psi_1^{\mathrm{h}} = \sum_{i=1}^{\infty} b_i r^{\mu_i} g_i(\vartheta) + \sum_{i=1}^{\infty} c_i r^{\bar{\eta}_i}\bar{h}_i(\vartheta). \tag{2.4b}$$

Here real parts are assumed and eigenvalues are ordered such that

$$\Re\{\bar{\lambda}_i\} < \Re\{\bar{\lambda}_{i+1}\}, \quad \Re\{\mu_i\} < \Re\{\mu_{i+1}\}, \quad \Re\{\bar{\eta}_i\} < \Re\{\bar{\eta}_{i+1}\}, \quad i \in \mathbb{N}.$$

A superscript 'h' refers to the solution of the unforced homogeneous problem, in which zero boundary conditions are applied on the two cones $\vartheta = \alpha, \beta$. The superscript 'p' refers to the particular integral which takes into account the rotation of the boundaries for Ω_0, and the forcing of the stream function Ψ_1 by Ω_0.

The homogeneous problems are responsible for the eigenmodes determined by the geometry. The eigenfunctions will serve as basis functions in the computational scheme and when the eigenfunctions of the meridional stream function are complex they represent eddies. For physical reasons we require that $\lambda_0 > 1$, $\bar{\lambda}_i > 1$, $\mu_i > 2$, and $\Re\{\bar{\eta}_i\} > 2$, for the flow to vanish in the corner $r \to 0$.

Once the Reynolds number is scaled out, the problem is completely specified by the parameters $(\alpha, \beta, \omega_1, \omega_2, \omega_3)$ and we shall investigate the flow behaviour across the full parameter space. However, we may exploit symmetry to reduce the parameter ranges by noting that the problem is symmetric under

$$(\alpha, \beta, \omega_1, \omega_2, \omega_3, \vartheta, \Psi, \Omega) \to (\alpha, \beta, -\omega_1, -\omega_2, -\omega_3, \vartheta, \Psi, -\Omega), \tag{2.5a}$$

$$(\alpha, \beta, \omega_1, \omega_2, \omega_3, \vartheta, \Psi, \Omega) \to (\pi - \beta, \pi - \alpha, \omega_2, \omega_1, \omega_3, \pi - \vartheta, \Psi, \Omega). \tag{2.5b}$$

Hence we assume without loss of generality that $0 \leqslant \alpha < \beta \leqslant \pi - \alpha$, and that the maximum value of the angular velocities ω_i is unity. In view of the non-dimensionalization this means we have

$$\max\{\omega_1, \omega_2, \omega_3\} = \max\{|\omega_1|, |\omega_2|, |\omega_3|\} = 1. \tag{2.6}$$

Symmetry issues are also explored in (**13**) and in particular the case of a symmetrical opening, when $\alpha = \pi - \beta$ and certain eigenfunctions are not present in the flow field. We shall not consider this case, and our general discussion applies to cones with asymmetrical openings.

2.1 *The $\mathcal{O}(1)$ problem*

We substitute the swirl and stream functions into the governing system of equations (2.1), and at leading order we require that

$$\mathbb{D}^2\Omega_0 = 0, \quad \Omega_0(r, \alpha) = \omega_1 r^2 \sin^2\alpha, \quad \Omega_0(r, \beta) = \omega_2 r^2 \sin^2\beta, \quad \Omega_0(1, \vartheta) = \omega_3 \sin^2\vartheta. \tag{2.7}$$

We consider first the particular integral Ω_0^{p}, taking the similarity form in (2.4a), chosen to satisfy no-slip boundary conditions on the cones. It is found that $\lambda_0 = 2$ and $f(\vartheta)$ satisfies

$$f_0'' - \cot\vartheta\, f_0' + 2 f_0 = 0, \quad f_0(\alpha) = \omega_1 \sin^2\alpha, \quad f_0(\beta) = \omega_2 \sin^2\beta, \tag{2.8}$$

where the prime denotes differentiation with respect to ϑ.

Equation (2.8) has the general solution

$$f_0(\vartheta) = \frac{1}{d_1}\left[(\omega_1 d_2 \sin^2\alpha + \omega_2 d_3 \sin^2\beta)\sin^2\vartheta + \sin^2\alpha\, \sin^2\beta\, (\omega_1 - \omega_2)\, \hat{f}_0(\vartheta)\right], \tag{2.9}$$

where $d_1(\alpha, \beta)$, $d_2(\alpha, \beta)$ and $d_3(\alpha, \beta)$ are known real constants depending on the chosen angles and $\hat{f}_0(\vartheta)$ is the function

$$\hat{f}_0(\vartheta) = \cos^2\vartheta\, \log((\cos\vartheta + 1)/(\cos\vartheta - 1)) + \log((\cos\vartheta - 1)/(\cos\vartheta + 1)) - 2\cos\vartheta.$$

For the homogeneous problem, $\mathbb{D}^2\Omega_0^{\rm h} = 0$ with zero boundary conditions on the cones, we use a change of coordinates $\vartheta = \alpha + \delta x$, $x \in [0,1]$, where $\delta = \beta - \alpha$, $f_i(x) = \bar{f}_i(\vartheta)$. We scale the eigenvalues $\bar{\lambda}_i = \lambda_i/\delta$ to ensure that they remain of order unity when the angular gap δ between the cones is small (see (**13**)). Henceforth a prime will denote differentiation with respect to x.

The resulting eigenvalue problem becomes

$$f_i'' - \delta\cot(\alpha+\delta x)\, f_i' + \lambda_i(\lambda_i - \delta)\, f_i = 0, \qquad f_i(0) = f_i(1) = 0. \tag{2.10}$$

We normalize the eigenfunctions with the condition $f_i'(0) = 1$. Computational solutions of this eigenvalue problem reveal that all eigenvalues and eigenfunctions are real and, for a fixed α, the $\bar{\lambda}_i$ decrease in magnitude (while the λ_i increase) with increasing β. Eigenvalues and eigenfunctions are shown in Fig. 2.

2.2 *The* $\mathcal{O}$(Re) *problem*

It can be seen from the governing equation (2.1) that the swirling motion $\boldsymbol{\Omega}_0$ induces a secondary, meridional circulation, and at $\mathcal{O}$(Re) the following equations are obtained:

$$\mathbb{D}^2\boldsymbol{\Omega}_1 = 0, \tag{2.11a}$$

$$\mathbb{D}^4\Psi_1 = \frac{2\boldsymbol{\Omega}_0}{r^2\sin^2\vartheta}\left(\cos\vartheta\,\frac{\partial\boldsymbol{\Omega}_0}{\partial r} - \frac{\sin\vartheta}{r}\,\frac{\partial\boldsymbol{\Omega}_0}{\partial\vartheta}\right), \tag{2.11b}$$

where the boundary conditions for Ψ_1 are given by (2.2b). Since $\boldsymbol{\Omega}_1$ satisfies the same eigenvalue problem as $\boldsymbol{\Omega}_0^{\rm h}$ and neither influences Ψ_1 nor has a major impact on the swirl function when Re $\ll 1$, we shall not pursue this solution any further.

The leading term of the stream function, Ψ_1, is decomposed in a similar manner to the swirl function into two components as indicated in (2.4b). The particular integral $\Psi_1^{\rm p}$ is driven by the swirling flow through the weak inertial terms that are quadratic in $\boldsymbol{\Omega}_0$, with zero boundary conditions

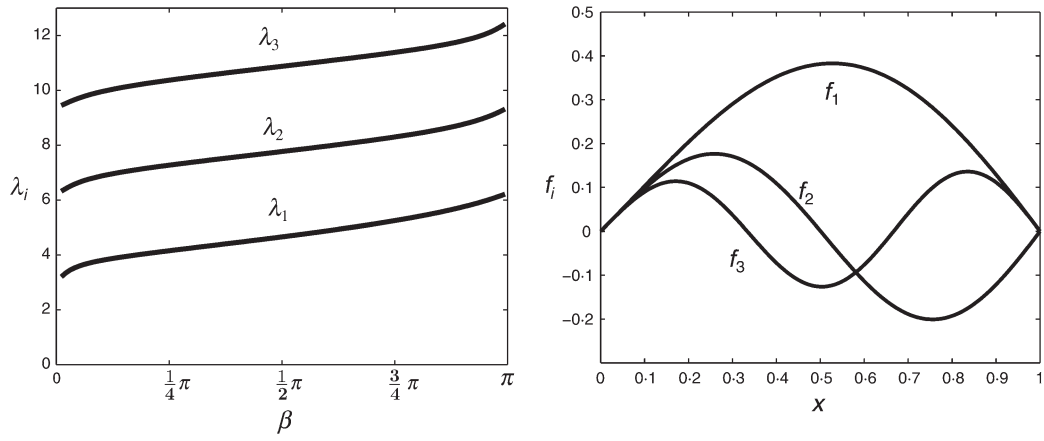

Fig. 2 The plot to the left shows the first three (real) eigenvalues λ_i plotted against the outer angle β for a fixed inner angle, $\alpha = 1^\circ$. To the right are plotted the three first eigenfunctions $f_i(x)$ for $\alpha = 30^\circ$ and $\beta = 60^\circ$

on the cones. The solution to the homogeneous, unforced equation Ψ_1^{h} is included to enforce zero meridional flow on the lid.

The homogeneous problem has been treated extensively in (**14**), following the approach in (**4**, **7**). The latter authors treated a single cone and showed that, with a change of variable $t = \cos\vartheta$, the eigenfunctions can be expressed as Legendre functions of the first kind whose degrees correspond to the eigenvalues. With the same change of variable for the double cone configuration, the eigenrelation is simplified considerably and the eddy functions can be expressed analytically in terms of known special functions. However, it is more convenient for our purposes of solving the complete forced problem to retain a formulation in terms of x; this will prove beneficial from a numerical perspective.

2.3 *Eigenfunctions for the meridional flow*

We begin by considering the homogeneous component of the leading-order meridional flow and use an expansion given by (2.4b). Setting $\bar{\eta}_i = \eta_i/\delta$, $\bar{h}_i(\vartheta) = h_i(x)$ gives the eigenproblem

$$\begin{aligned}
&\eta_i(\eta_i-\delta)(\eta_i-2\delta)(\eta_i-3\delta)h_i(x)\\
&\quad-\delta\cot(\alpha+\delta x)[(\eta_i-2\delta)(\eta_i-3\delta)+\eta_i(\eta_i-\delta)+3\delta^2+3\delta^2\cot^2(\alpha+\delta x)]h_i'(x)\\
&\quad+[(\eta_i-2\delta)(\eta_i-3\delta)+\eta_i(\eta_i-\delta)+3\delta^2\cot^2(\alpha+\delta x)]h_i''(x)\\
&\quad-2\delta\cot(\alpha+\delta x)h_i'''(x)+h_i''''(x)=0,
\end{aligned}\tag{2.12}$$

with boundary conditions $h_i(0) = h_i(1) = h_i'(0) = h_i'(1) = 0$ from (2.2b), accompanied by a normalization condition, $h_i''(0) = 1$. Equation (2.12) can be solved numerically, as described in section 3, to find the eigenvalues η_i.

Computation of the eigenrelation reveals that for a small opening δ between the cones, regardless of the value of $\alpha < \pi$, all eigenvalues and eigenfunctions are complex. A similar pattern is observed for a wedge geometry (**1**) or a single cone (**5** to **7**). From the eigenrelation it follows that eigenvalues occur as complex conjugate pairs, ensuring that the stream function is real-valued, and we shall therefore only consider eigenvalues with positive imaginary part. In passing we also observe that for specified angles α and β, similar to other geometries (see, for example, (**6**)), $\Re(\eta_{i+1}-\eta_i)$ tends to a constant ($\approx \pi$) for increasing i, but since we are interested in the leading eigenvalues we do not aim to obtain an expression for the asymptotic behaviour of the eigenvalues.

Now suppose that the inner cone angle is fixed and small, $0 < \alpha \ll 1$. As the outer cone angle β is increased from α, we reach a critical value β_{c} where a bifurcation occurs. The pair of complex conjugate eigenvalues with the smallest real part bifurcates into two real eigenvalues. Near the apex of the cone, the flow is dominated by the mode associated with the eigenvalue possessing the smallest real part. Thus, when the flow is driven by a far-field disturbance, this bifurcation would signal the disappearance of an infinite sequence of eddies near the apex. As β is further increased, further bifurcations occur, however, the dominant eigenvalue remains real and hence we shall focus only on the first bifurcation point.

In contrast to the single-cone geometry, for the double-cone geometry we study, the critical angle β_{c} is a function of the inner cone angle α. It is found that the critical angle $\beta_{\mathrm{c}}(\alpha)$ increases with increasing α until a point is reached where $\alpha = \alpha_{\mathrm{nc}} \simeq 78^\circ$, at which $\beta_{\mathrm{c}} = \pi$. For angles α greater than α_{nc}, the dominant eigenvalue $\bar{\eta}_1$ remains complex over the whole admissible range of β.

We have considered cone geometries throughout the whole of the (α, β) domain. Hewitt (**13**) and Malhotra *et al.* (**14**) give results for the eigenvalue distribution for specific choices of angles. Our computed results of the eigenrelation show an excellent agreement with the particular results in (**13**, **14**) and these papers provide a reliable check upon our numerical scheme.

Instead of focusing on particular values of α and β, we map the behaviour of the leading eigenvalue $\bar{\eta}_1$ across the (α, β) plane. Figure 3 shows the real part (left) and imaginary part (right) in the plane. The region $\alpha \geqslant \beta$ is unphysical and so excluded, and there is a reflection symmetry about the line $\beta = \pi - \alpha$ as expected from the symmetry relations (2.5). On the right-hand plot there is a clear transition from real to complex eigenvalues, and this is shown as a dashed line $\beta = \beta_c(\alpha)$ on the summarizing Fig. 4. We observe a steep decline in β_c as $\alpha \to 0$. Note that for a single, outer cone and no inner cone the critical angle is $\beta_c \simeq 81^\circ$, while for two cones and a very thin inner cone, say $\alpha = 0{\cdot}5^\circ$, the critical angle $\beta_c \simeq 106^\circ$. Note that Fig. 3 is in the thesis of Hynes (**15**), but not as far as we know in the published literature. Figure 4 is both in this thesis and is presented by Moffatt (**17**).

2.4 *The forced meridional flow*

We now return to the inhomogeneous problem. The dominant meridional flow component in (2.4b) arises from the exponents with the smallest real part; it can either be due to the eigenvalue $\bar{\eta}_1$ arising from the homogeneous component Ψ_1^{h}, that is, from the geometry, or the first exponent μ_1 from the forced term Ψ_1^{p}.

In the governing differential equation for Ψ_1^{p}, the inertial terms give a component that is quadratic in $\boldsymbol{\Omega}_0$. From (2.4b) and (2.11b) each exponent μ_i of the forced component is equal to the sum of the exponents from any two non-zero terms in the expansion (2.4a) for $\boldsymbol{\Omega}_0$ plus 1. All these exponents are real, note, and so cannot give rise to an infinite sequence of eddies.

In general for the cases 2 and 3 (in which the cones rotate), the term with exponent $\lambda_0 = 2$ is present in (2.4a) for $\boldsymbol{\Omega}_0^{\mathrm{p}}$ and is found to be dominant in $\boldsymbol{\Omega}_0$. With stationary cones and a rotating lid (case 1), this term is not present ($a_0 = 0$) and so the leading eigenvalue $\bar{\lambda}_1$ in $\boldsymbol{\Omega}_0^{\mathrm{h}}$ is most significant.

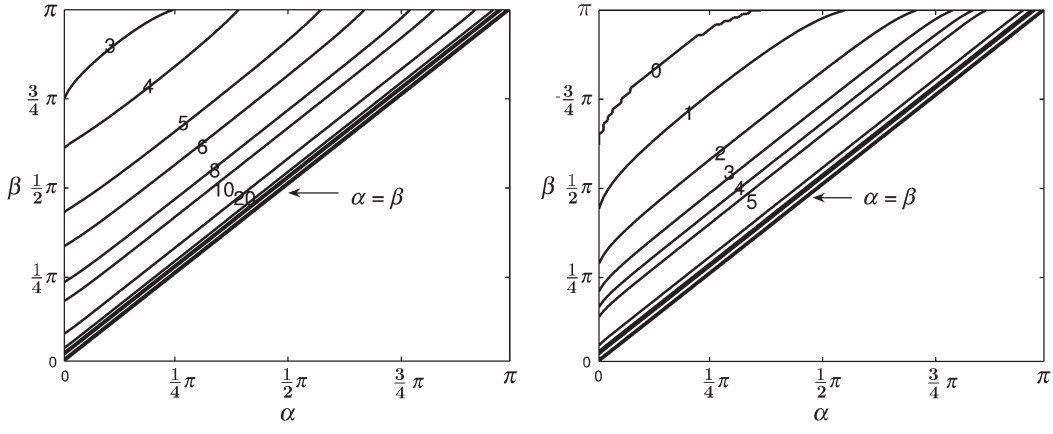

Fig. 3 Plotted are the real (left) and imaginary (right) parts of $\bar{\eta}_1$ as a function of (α, β). The contour levels are as indicated in the figures and thereafter increase in steps of ten

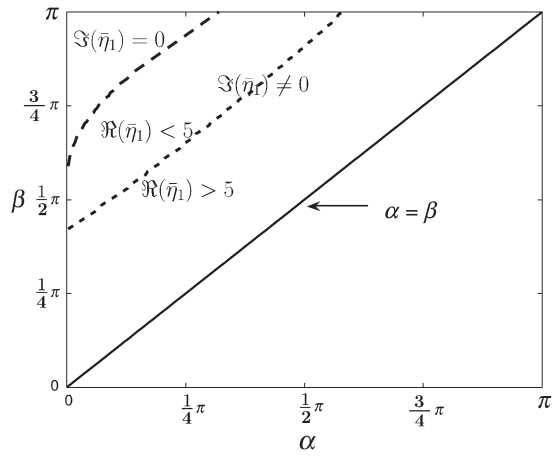

Fig. 4 The dashed line indicates the border between complex and real values of $\bar{\eta}_1$ in the (α, β) plane. The dotted line indicates when $\Re(\bar{\eta}_1) = 5$

In summary, we have

$$\mu_1 = \begin{cases} 2\bar{\lambda}_1 + 1, & \text{case 1,} \\ 2\lambda_0 + 1 = 5, & \text{cases 2 and 3.} \end{cases}$$

We can therefore make a prediction about when there will exist an infinite sequence of toroidal vortices near the apex. In cases 2 and 3 we require that $\bar{\eta}_1$ is complex and dominant, $\Re(\bar{\eta}_1) < \mu_1 = 5$. In case 1, we would require that $\bar{\eta}_1$ is complex and dominant so that $\Re(\bar{\eta}_1) < \mu_1 = 2\bar{\lambda}_1 + 1$. However, according to our numerical investigations this latter inequality holds true for all angles α and β and so may be dropped. Thus the condition for an infinite sequence of eddies to occur becomes

$$\begin{aligned} &\Im(\bar{\eta}_1) > 0, && \text{case 1,} \\ &\Im(\bar{\eta}_1) > 0,\ \Re(\bar{\eta}_1) < 5, && \text{cases 2 and 3.} \end{aligned} \tag{2.13}$$

In Fig. 4 we use our numerical results to translate these conditions into the (α, β) plane. The dashed line separates the two regions where $\bar{\eta}_1$ is complex and real, the complex domain lying to the right of the dashed curve. In case 1 (rotating lid) a sequence of eddies would generally be present at points (α, β) to the right of this curve. The dotted curve in the figure indicates $\Re(\bar{\eta}_1) = 5$ (with values exceeding 5 on the right of the curve). In cases 2 and 3 of rotating cones we can only expect eddies if the angles (α, β) give a point between the dashed and dotted curves.

In section 4 we shall investigate under which circumstances sequences of toroidal eddies can be observed in the geometry. However, first of all we present our numerical methods in more detail.

3. Computational methods

We follow a similar approach to (**18**) in which the Moffatt eddy functions serve as basis functions for a truncated sum and the unknown coefficients are found through collocation. The infinite series

(2.4) are truncated to N terms each. We anticipate from the results in (**18**) that even when N is small and just a few basis functions are used, the dominant flow features will be clearly visible and will not change significantly when N increases. At the intersection of lid and cones there will typically be discontinuities in the angular velocities. These corner singularities have little impact on the global flow (**19**). However, they cause numerical oscillations near the lid. An increased number of basis functions reduces the magnitude of the oscillations and hence improves the flow visualization. As an experimentally determined choice we set $N = 50$.

Our computations follow a scheme consisting of five steps. First solutions to the eigenrelations (2.10) and (2.12) governing Ω_0^{h} and Ψ_1^{h} in (2.4) are computed, using a second-order finite difference scheme. The first 15 eigenvalues and eigenfunctions are refined using Matlab's boundary-value problem solver `bvp4c` to obtain an accuracy of 10^{-10}. Next, the particular solution of Ω_0^{p} in (2.4) is computed from (2.8) and although an exact solution exists (2.9) it is more convenient to compute the solution with a shooting method. Then the no-slip condition on Ω_0 in (2.7) on the spherical lid at $r = 1$ determines the coefficients a_i in the expression (2.4) for Ω_0^{h}.

Each term of the forced part of the stream function has a quadratic dependence on the basis functions of the swirl. In the fourth step of the numerical scheme, we seek the N first terms of Ψ_1^{p} in (2.4) ordered by the magnitude of the exponent μ_i, starting with the smallest. Each term $b_i r^{\mu_i} g_i(\vartheta)$ is computed using a finite difference method. The sum of the forced part Ψ_1^{p} and the homogeneous part Ψ_1^{h} of the stream function must obey the no-slip boundary condition (2.3) on the lid, and the final step uses this condition to fix the coefficients c_i in (2.4).

3.1 *A comparison of collocation schemes*

To determine the coefficients a_i and c_i we have used the collocation scheme used by Hills (**18**). This method implements the boundary conditions at N uniformly distributed points along the lid,

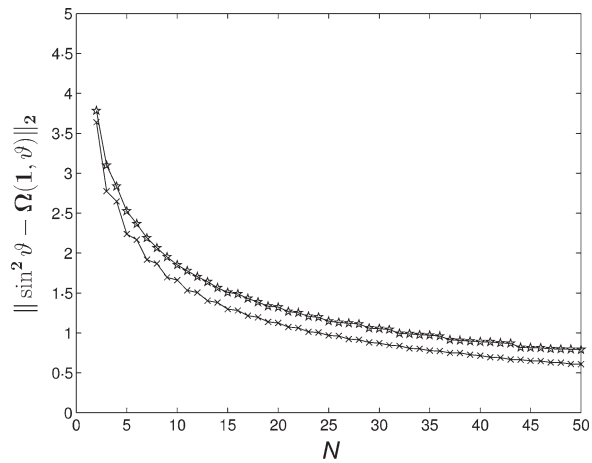

Fig. 5 The norm of the residual for the swirl function with an increasing number of basis functions. The lower curve plotted with crosses is for Shankar's method while the curve plotted with stars shows Hills's collocation scheme

avoiding the end points where there are discontinuities. Another, least squares method has been developed by Shankar (**6**), which has the benefit of giving the residual with minimal 2-norm over a number of mesh points that can be increased to exceed the number of basis functions; in what follows we have used $5N$ mesh points.

Figure 5 shows the norm of the residual, measured in discretized 2-norm, against the number N of basis functions, for the two methods when applied to a rotating lid with stationary cones. As expected the least squares method gives a smaller residual for any value of N. The slow decrease in residual stems from the fact that we impose the boundary conditions (2.10) which result in discontinuities at the end points. However, the collocation scheme of Hills has the benefit of giving less oscillatory results as well as resulting in a smaller condition number for the computational matrix. In Fig. 6 we display the computed residual for the swirl function at the lid for both methods with $N = 10,\ 20$ and 50. We see that Shankar's method is far more oscillatory along the lid while it gives a better approximation near the end points and hence gives a smaller total residual. We can also see Gibbs's phenomenon at the end points.

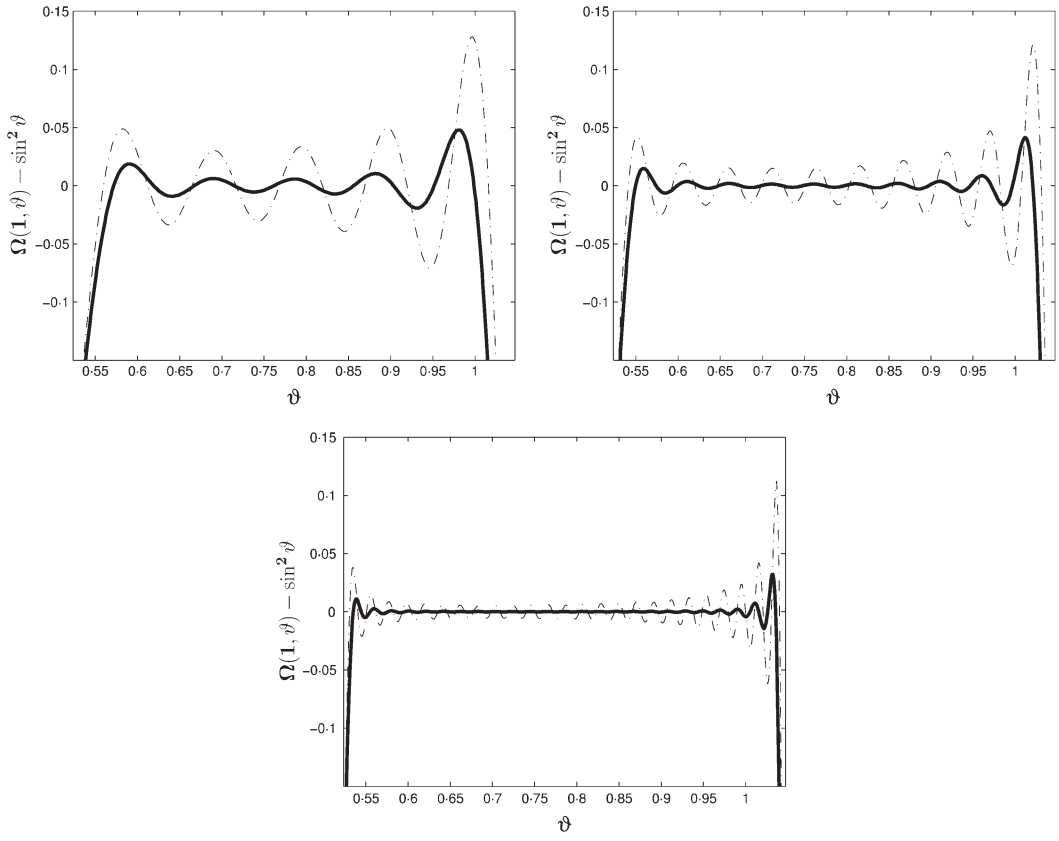

Fig. 6 The residual at each point on the lid for the swirl function for $N = 10, 20, 50$. The dash–dotted line shows the residual for Shankar's method while the thick solid line shows residual for Hills's collocation scheme

We find that the least squares method does not work well for combined Dirichlet and Neumann conditions and so for the stream function with boundary conditions (2.3) we need to use the collocation method. We plot the residual for the stream function at the lid against the number of eigenfunctions used in the computational scheme. As can be seen in Fig. 7, the residual decreases with an increased number of basis functions. The convergence is substantially faster than for the swirl as we do not have any discontinuities. The eigenfunctions constituting the basis of Ψ_1^{h} are not known to be complete. However, the decreasing residual shows that the representation is sufficient for our need of describing the flow. In Fig. 8 we show how the residual decreases with an increased number of basis functions.

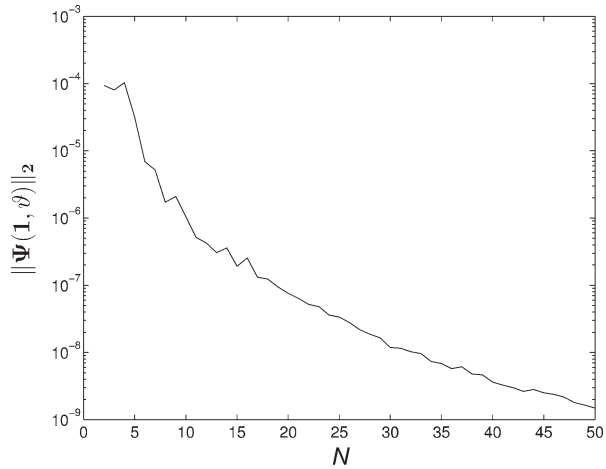

Fig. 7 The norm of the residual of the stream function at the lid with an increasing number of basis functions computed with the collocation scheme

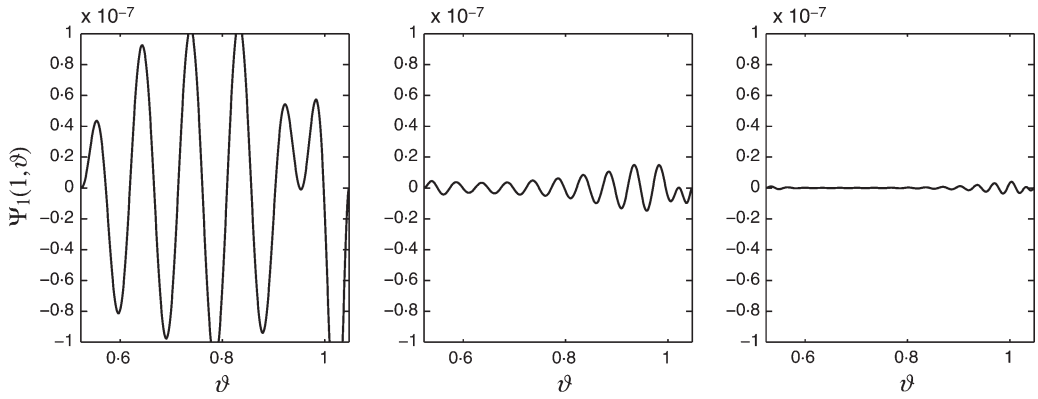

Fig. 8 The residual of the stream function at the lid for $N = 10, 20, 30$ computed with Hills's collocation scheme

The results were checked against those of Hewitt (**13**), computed with a finite difference method, and excellent agreement was obtained.

4. Results

In this section we examine the computed results for the swirl and stream functions for different parameter values. In passing, we note that the swirl function can be written as a linear combination of flows driven by the three angular velocities of the boundaries,

$$\Omega_0(r,\vartheta) = \omega_1\tilde{\Omega}_1(r,\vartheta) + \omega_2\tilde{\Omega}_2(r,\vartheta) + \omega_3\tilde{\Omega}_3(r,\vartheta),$$

where $\tilde{\Omega}_i$ is forced by the motion of just one of the three boundaries. Since the leading-order term of the stream function, Ψ_1, has a quadratic dependence on the terms in $\boldsymbol{\Omega}$, it follows that Ψ_1 can be written as a sum of six components:

$$\begin{aligned}\Psi_1(r,\vartheta) = {}& \omega_1^2\tilde{\Psi}_{1,1}(r,\vartheta) + \omega_2^2\tilde{\Psi}_{2,2}(r,\vartheta) + \omega_3^2\tilde{\Psi}_{3,3}(r,\vartheta)\\ &+ 2\omega_1\omega_2\tilde{\Psi}_{1,2}(r,\vartheta) + 2\omega_2\omega_3\tilde{\Psi}_{2,3}(r,\vartheta) + 2\omega_3\omega_1\tilde{\Psi}_{3,1}(r,\vartheta),\end{aligned}$$

with $\tilde{\Psi}_{i,j}(r,\vartheta)$ denoting the part forced by $\tilde{\Omega}_i$ and $\tilde{\Omega}_j$. Any meridional flow generated through rotation can be described by these six terms.

This set of nine fields $\tilde{\Omega}_i$ and $\tilde{\Psi}_{i,j}$ is sufficient to describe the response to any driving. The choice of basis here is somewhat arbitrary. An alternative representation is to express the controlling parameters $(\omega_1,\omega_2,\omega_3)$ as a linear combination of the vectors $(1,1,1)$, $(1,-1,0)$ and $(0,0,1)$, where the first vector corresponds to rigid-body rotation, the second to shear between the upper and lower cone and the third to just a rotating lid. If we write

$$(\omega_1,\omega_2,\omega_3) = \omega_{\rm rot}(1,1,1) + \omega_{\rm sh}(1,-1,0) + \omega_{\rm lid}(0,0,1)$$

then we have

$$\Omega_0(r,\vartheta) = \omega_{\rm rot}\tilde{\Omega}_{\rm rot}(r,\vartheta) + \omega_{\rm sh}\tilde{\Omega}_{\rm sh}(r,\vartheta) + \omega_{\rm lid}\tilde{\Omega}_{\rm lid}(r,\vartheta).$$

We note that $\tilde{\Omega}_{\rm rot} = r^2\sin^2\vartheta$ is rigid-body rotation and $\tilde{\Psi}_{\rm rot} = 0$ since a rigid-body rotation does not drive a meridional flow from (2.11b). Hence, the stream function may be expressed as a sum of five terms:

$$\Psi_1 = \omega_{\rm sh}^2\tilde{\Psi}_{\rm sh} + \omega_{\rm lid}^2\tilde{\Psi}_{\rm lid} + 2\omega_{\rm rot}\omega_{\rm sh}\tilde{\Psi}_{\rm rot,sh} + 2\omega_{\rm sh}\omega_{\rm lid}\tilde{\Psi}_{\rm sh,lid} + 2\omega_{\rm lid}\omega_{\rm rot}\tilde{\Psi}_{\rm lid,rot}.$$

4.1 *Flows*

For the visualization of the flows we shall consider a specific choice of angles: henceforth in this subsection $\alpha = \pi/6$ and $\beta = \pi/3$. Our choice of acute angles is intentional in view of applications. We aim to work within the framework suggested above, starting with some basic flows and moving on to a general combination of them. In all the figures, stream line contours differ by a factor of a power of ten for the stream function Ψ_1, while for the swirl function Ω_0 the difference is 0·05. Dotted contour lines for the swirl function indicate negative values while positive are solid.

As a starting point, consider the flow driven by the rotation of the outer lid, $(\omega_{\rm rot},\omega_{\rm sh},\omega_{\rm lid}) = (0,0,1)$; this is case 1. In Fig. 9, contour lines of the swirl function and the meridional stream function in the (r,ϑ) plane are shown. As expected, the swirl decreases with the distance from the

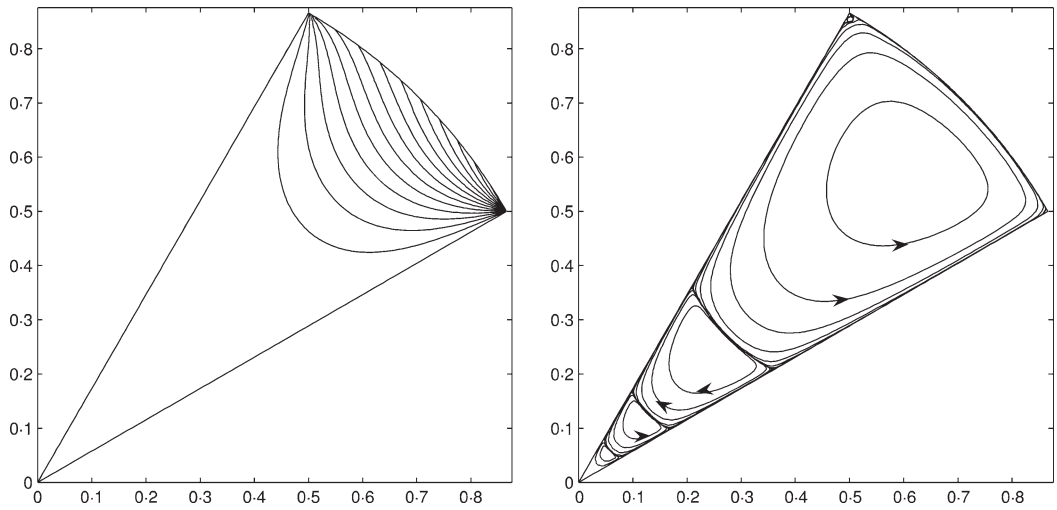

Fig. 9 Contours of the swirl function (left) and the stream function (right) when $\alpha = \pi/6$ and $\beta = \pi/3$, $(\omega_{\rm rot}, \omega_{\rm sh}, \omega_{\rm lid}) = (0, 0, 1)$

lid. In the absence of forced modes from rotation of the cones, the meridional flow is dominated by the first eigenmode for which $\bar{\eta}_1 \simeq 9{\cdot}64 + 4{\cdot}16i$, yielding an infinite sequence of counter-rotating toroidal vortices of descending strength towards the apex. In the figure we also indicate the directions of the eddies and note that the largest eddy near the lid is rotating counter-clockwise corresponding to positive real values of the stream function.

The behaviour of the stream function corresponds well with the results of Hewitt (**13**), in that the slowest decaying eigenmode dictates the behaviour for most of the flow domain. Hence, the curvature exhibited by higher-order eigenmodes indicated in (**14**) is not visible. When the apex is approached the strength of eddies decays geometrically. Moffatt (**1**) derived an expression for this common fall-off ratio

$$C = \exp\left(\frac{\pi\,\bar{\eta}_1^{\rm re}}{\bar{\eta}_1^{\rm im}}\right), \quad \bar{\eta}_1 = \bar{\eta}_1^{\rm re} + i\,\bar{\eta}_1^{\rm im}; \tag{4.1}$$

in this case $C \simeq 1450$.

In Fig. 10 we show the swirl and the stream function in the case of shearing cones and a stationary lid, $(\omega_{\rm rot}, \omega_{\rm sh}, \omega_{\rm lid}) = (0, 1, 0)$; this is an example of case 2. The cones, rotating in opposite directions, induce meridional circulations of opposite signs. The stream function consists of two parts, circulating in opposite directions. The region emanating from the outer cone is circulating clockwise and is much larger than the part induced by the inner cone due to the greater centrifugal effect. The apex is void of toroidal vortices as the forced mode is dominant over the first eigenmode, $\Re(\bar{\eta}_1) > 5$; see (2.13).

Our third choice of rotation, rigid-body rotation, is of little interest as it does not induce any secondary meridional circulation. Instead, in Fig. 11 we consider a general combination of the three rotations and let $(\omega_{\rm rot}, \omega_{\rm sh}, \omega_{\rm lid}) = (1/4, 3/4, 1/4)$ or $(\omega_1, \omega_2, \omega_3) = (1, -1/2, 1/2)$; this is case 3. The forcings from the cones are of the same magnitude, $|\omega_1 \sin^2\alpha| = |\omega_2 \sin^2\beta|$ leading

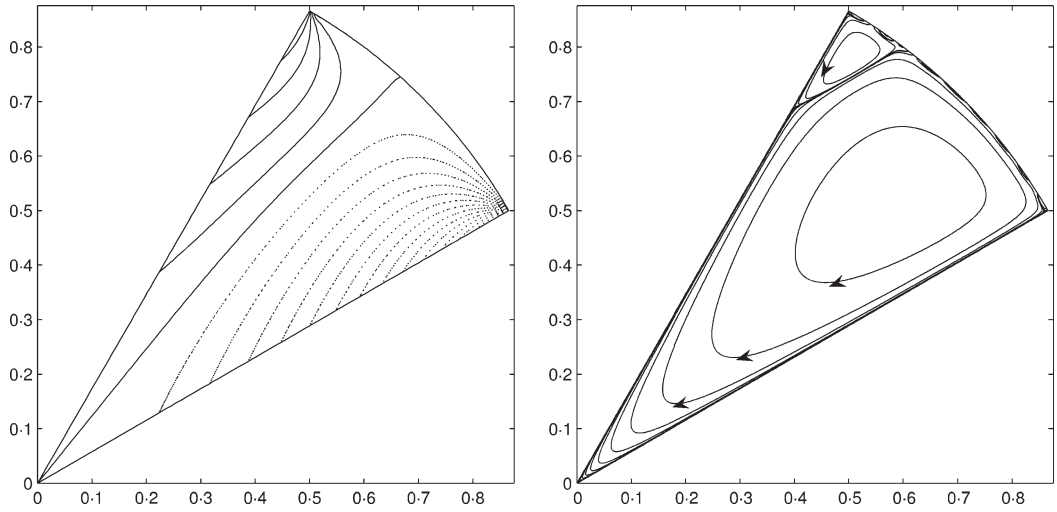

Fig. 10 Contour lines of the swirl function (left) and the stream function (right) when $\alpha = \pi/6$ and $\beta = \pi/3$, case 2 with $\omega_1 = 1$ and $\omega_2 = -1$

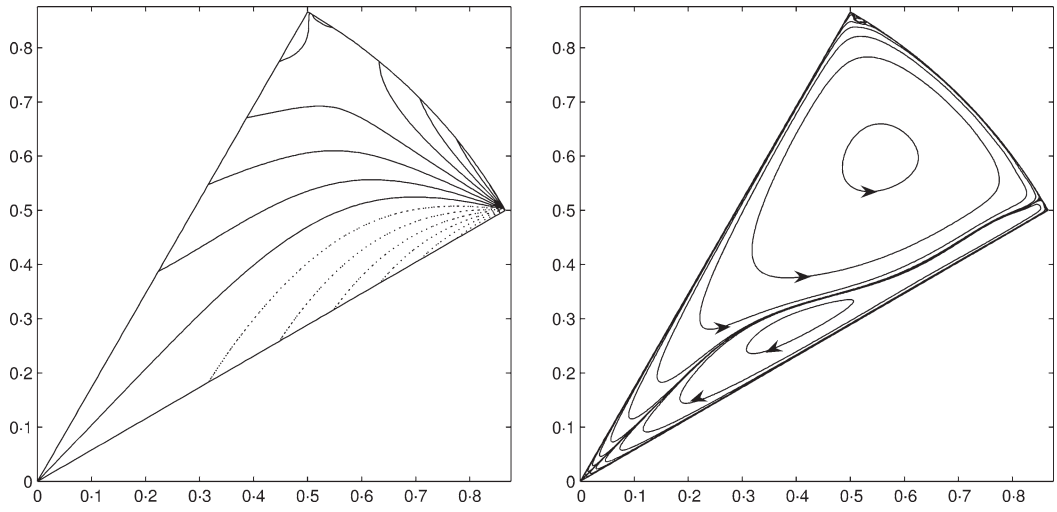

Fig. 11 Contours of the swirl function (left) and the stream function (right) when $\alpha = \pi/6$ and $\beta = \pi/3$, case 3 with $(\omega_1, \omega_2, \omega_3) = (1, -1/2, 1/2)$

to the presence near the apex, again void of eddies, of two circulatory regions of opposite signs in a symmetric flow region around the centre-line. The forcing from the lid has little effect on the structure of the flow near the apex but as we move further away from the apex, the influence from the lid becomes notable. The rotation of the inner cone and the lid induce a meridional stream function

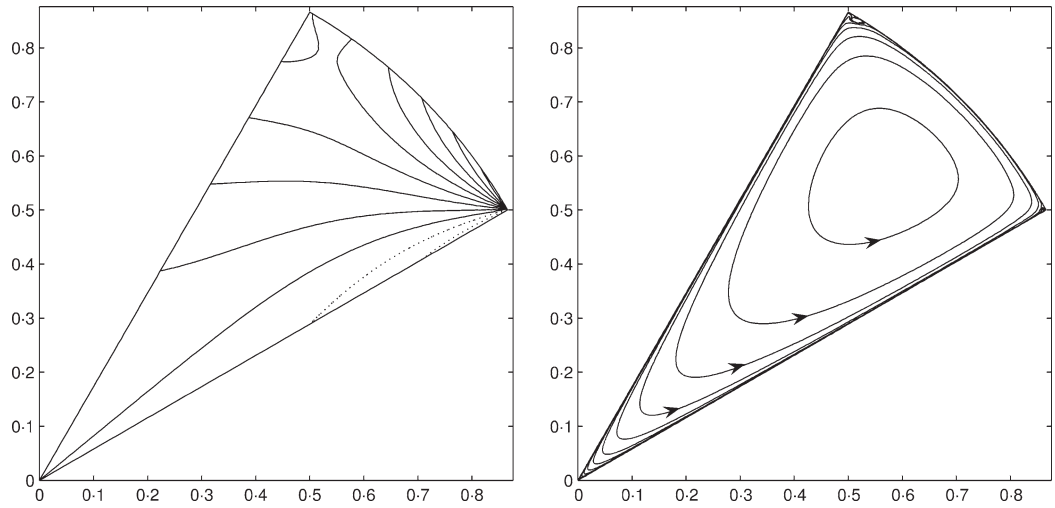

Fig. 12 Contours of the swirl function (left) and the stream function (right) when $\alpha = \pi/6$ and $\beta = \pi/3$, case 3 with $(\omega_1, \omega_2, \omega_3) = (1, -1/5, 3/5)$

of counter-clockwise orientation; the eddy with clockwise circulation, dominant in Fig. 10, has been pushed towards the outer cone where it is generated.

In Fig. 12 the stream function consists of a single circulatory region, the driving equals $(\omega_{\text{rot}}, \omega_{\text{sh}}, \omega_{\text{lid}}) = (2/5, 3/5, 1/5)$. The contribution to the stream function from the forcing of the inner cone combined with forcing of the lid dominates over the part induced by the outer cone. The counter-clockwise circulation fills the entire flow domain. Again, there are no vortices in the apex forced by the swirl.

4.2 *Toroidal vortices*

In the examples in the previous section we observed that rotating the cones could destroy the infinite sequence of Moffatt eddies obtained by driving the lid alone. However, from the analysis in section 2.3 we conclude that for certain values of α and β, when the second case of (2.13) is satisfied (as illustrated in Fig. 4), toroidal vortices will appear near the apex even when the motion is driven by the rotation of the cones, cases 2 and 3, and not just the lid, as discussed in (**15**, **17**).

Although theoretical considerations predict an infinite eddy sequence in this case, the visualization of this is far from straightforward. The first reason is that when $\Re\{\bar{\eta}_1\} < 5$ the difference in (2.4) between the exponent μ_1 of the leading forced mode and the real part of the exponent of the leading eigenmode is typically small. The other reason is the rapid, geometric, spatial decay rate of the eddies. Both the imaginary and the real parts of the eigenvalues $\bar{\eta}_i$ decrease with an increased cone opening. If the first eigenmode is complex and clearly dominant over the first forced mode as $r \to 0$, the imaginary part will be small and therefore, according to (4.1), increase the rate with which the eddies fall off. Hence the size of the recirculatory region will be close to the numerical accuracy of the computational scheme. On the other hand, choosing angles such that $\Im\{\bar{\eta}_1\} > 1$, the difference between μ_1 and $\Re\{\bar{\eta}_1\}$ will be small and the latter will not dominate until very near the apex.

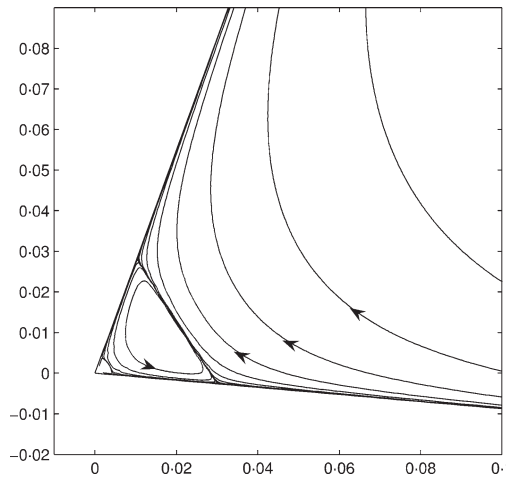

Fig. 13 Eddies induced by the rotation of the outer cone since for $\alpha = 20^\circ$, $\beta = 95^\circ$, the most slowly decaying mode is actually an eigenmode with $\bar{\eta}_1 \simeq 4{\cdot}89 + 1{\cdot}35i$ and not a forced mode

Figure 13 shows the computed stream function zoomed near the apex when $\alpha = 20^\circ$ and $\beta = 95^\circ$, with $\bar{\eta}_1 \simeq 4{\cdot}89 + 1{\cdot}35i$. The motion is driven by the rotation of the outer cone, $(\omega_1, \omega_2, \omega_3) = (0, 1, 0)$, and an eddy is clearly visible with a decay factor $C \simeq 8{\cdot}4 \times 10^4$.

An interesting feature of the existence of eddies is related to symmetries. Hewitt (**13**) showed that for a symmetric cone opening $\alpha = \pi - \beta$ the forcing from the lid in case 1 does not excite the leading complex eigenmode with exponent μ_1 in Ψ_1. Hence in this case, the flow is dominated by the first driven mode, leaving the apex void of toroidal vortices despite the slowest decaying mode being complex and the first condition in (2.13) being satisfied.

Interestingly enough, the reverse situation may also occur, where due to symmetries the first forced mode cancels out and the flow is dominated by the first eigenmode giving a sequence of eddies, even though its exponent is larger and (2.13) is not satisfied. The symmetry here, however, is due to the driving from the cones. In Fig. 14, we display the stream function for $\alpha = 20^\circ$ and $\beta = 75^\circ$, in which the motion is driven by the rotation of the cones with $(\omega_1, \omega_2, \omega_3) = (1, 1, 0)$. The first eigenvalue $\bar{\eta}_1 \simeq 6{\cdot}05 + 2{\cdot}07i$ and we would not expect an eddy structure near the apex, nevertheless, in Fig. 14 a sequence of eddies is clearly visible there. The explanation for this behaviour is found from the form of (2.9); the equal rotation rates of the cones cancel the second term of the particular solution of $\mathbf{\Omega}_0$ and the right-hand side for the first term of (2.11b) becomes zero. In other words, the symmetric forcing of the cones does not excite the first forced mode. Instead, the first eigenmode, whose real part is smaller than the second forced term, dominates, giving rise to a sequence of eddies with fall-off ratio $C \simeq 9{\cdot}5 \times 10^3$.

4.3 *Closed regions*

We have seen that depending on the driving of the flow in the conical geometry we consider, the number of meridional eddies can vary from one to infinity. In mixing applications it is generally desirable to have just one eddy in the fluid flow. In this case rapid mixing occurs along streamlines

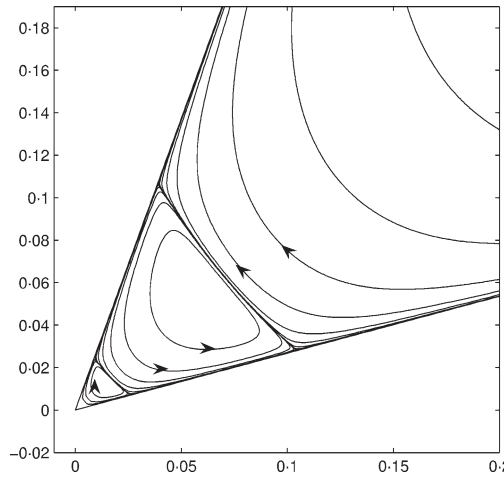

Fig. 14 Eddies appearing due to symmetric forcing when $\alpha = 20^\circ$, $\beta = 75^\circ$, $\bar{\eta}_1 \simeq 6{\cdot}05 + 2{\cdot}07i$, $(\omega_1, \omega_2, \omega_3) = (1, 1, 0)$

by the shear–diffuse mechanism followed by slower mixing across stream lines and separatrices (**20**, **21**). Time dependence can increase the rate of mixing by making the flow chaotic. Separatrices are generally undesirable for mixing processes as they separate distinct eddies, and also link to the boundary layers where the motion is sluggish and mixing poor. Although we have not tried to introduce time dependence, nor have we tried to simulate and quantify the mixing of a diffusing passive scalar, we have scanned parameter space to understand how the number of eddies depends on the driving of the flow and so classify flow topology as a prelude to a more detailed study.

A change of sign in the stream function Ψ_1 signals the presence of a separatrix in the flow. We can obtain the number of closed regions in the flow by scanning over the parameter space of rotation rates $(\omega_1, \omega_2, \omega_3)$ for a specified cone opening (α, β), and counting the number of maxima and minima in the stream function in each case.

Obtaining a quantitative picture of the number of separate eddy regions as a function of (α, β) and the three rotation rates would be difficult. However, from our scaling of the rotation rates (2.6) we reduce the problem to four parameters, so that for a given cone opening we are able to display the behaviour for arbitrary rotation rates. Hence we shall focus on two representative choices of cone geometry to indicate how the number of separatrices changes for different parameter values.

In Fig. 15 we display the number of separate regions when one rotation rate is kept constant at unity while the other two are varied from -1 to 1. The darker the colour the larger is the number of closed regions found in the flow, and white areas indicate that the meridional flow contains no separatrices for the chosen parameter values. We observe between one and four eddies numerically, but will point out when an infinite sequence should actually be present.

In Fig. 15(a), the lid rotation rate ω_3 is kept constant for $\alpha = 30^\circ$ and $\beta = 60^\circ$ while the cone rotation rates ω_1 and ω_2 are varied. The case when the cones are held stationary (Fig. 9) corresponds to the origin of the figure. We have already shown that an infinite sequence of eddies exists for this driving and as expected the largest number, four, of closed regions are found near this point. It is interesting to note that along the line $\omega_1 = \omega_2$ the number of closed regions remains large because

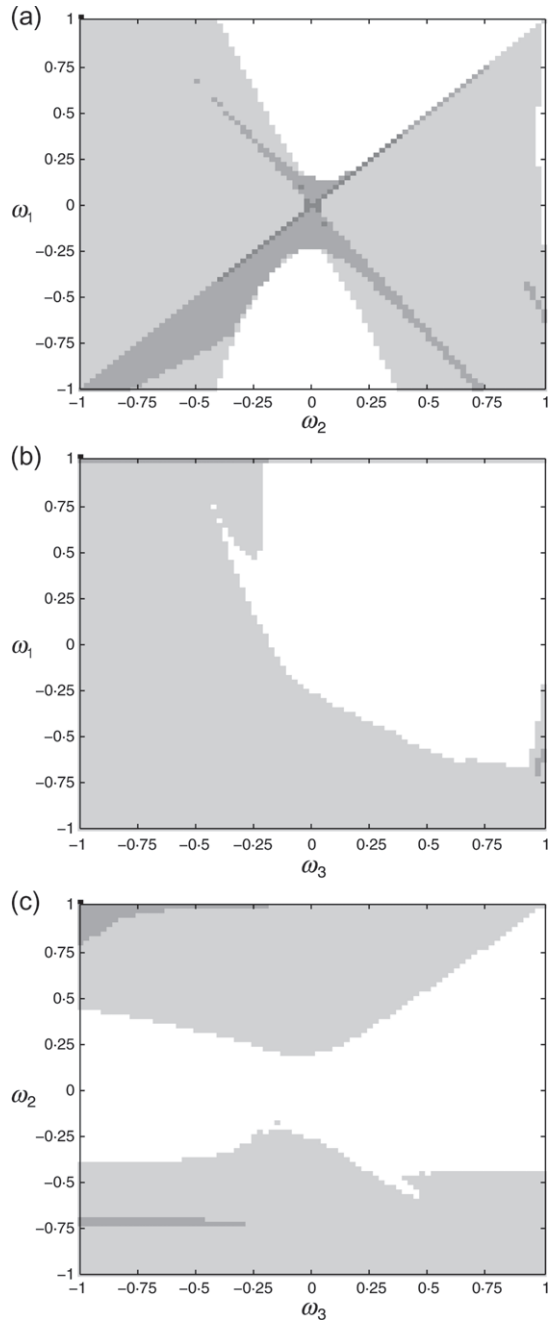

Fig. 15 The number of circulatory regions present in the meridional stream function as a function of (a) (ω_1, ω_2) for $\omega_3 = 1$, (b) (ω_1, ω_3) for $\omega_2 = 1$, (c) (ω_2, ω_3) for $\omega_1 = 1$. The cone geometry is given by $\alpha = 30^\circ$ and $\beta = 60^\circ$ and the number of eddies is plotted by pixels varying from white (one eddy) to black (four eddies)

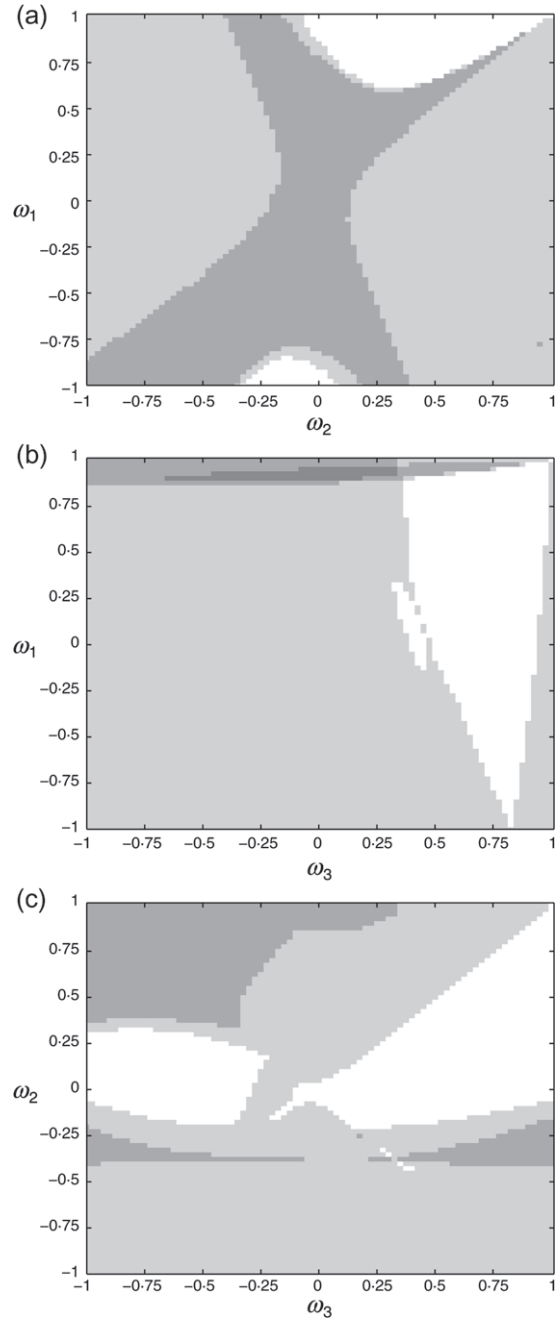

Fig. 16 The number of circulatory regions present in the meridional stream function as a function of (a) (ω_1, ω_2) for $\omega_3 = 1$, (b) (ω_1, ω_3) for $\omega_2 = 1$, (c) (ω_2, ω_3) for $\omega_1 = 1$. The cone geometry is given by $\alpha = 20^\circ$ and $\beta = 75^\circ$ and the number of eddies is plotted by pixels varying from white (one eddy) to black (four eddies)

of the form of (2.9) discussed above; essentially this corresponds to adding a solid-body rotation to the system.

Figure 15(b) shows the number of separatrices in the flow when the outer cone is kept at a constant rotation rate $\omega_2 = 1$ with $\alpha = 30^\circ$ and $\beta = 60^\circ$. We do not expect a Moffatt eddy structure from this driving and for most of the parameter range only one or two closed regions are present in the flow. In Fig. 15(c) ω_1 is held constant.

For a different cone opening the results show some notable changes. In Fig. 16(a) $\omega_3 = 1$ but the angles are now given by $\alpha = 20^\circ$ and $\beta = 75^\circ$. We see that the region when the flow contains separatrices is greater than for the previous cone opening. Near the origin of Fig. 16(a) when the flow is driven only by the lid, there will be an infinite sequence of eddies, of which we resolve only the first three. Moving away from the origin the number of eddies generally decreases.

In Fig. 16(b) an infinite sequence of eddies occurs on the top boundary, that is, when $\omega_1 = \omega_2$; we see up to four of these eddies (because of the limitation of the numerical accuracy we see an increased number of eddies when ω_1 is slightly less than one). This is the effect from symmetry discussed previously and shown in Fig. 14: for the symmetric driving the first forced mode cancels out and the first eigenmode with exponent $\bar{\eta}_1 \simeq 6{\cdot}05 + 2{\cdot}07i$ dominates near the apex. When $\omega_1 = 1$, shown in Fig. 16(c), the number of separatrices increases when ω_2 approaches the value of one for the same reason. By contrast, the infinite sequence does not appear in Fig. 15(b) because for this cone opening the real part of the first eigenmode with exponent $\bar{\eta}_1 \simeq 9{\cdot}64 + 4{\cdot}16i$ is still greater than that of the second forced mode.

5. Summary and outlook

We have investigated the low-Reynolds-number flow between two cones with coincident apices enclosed by a spherical lid, where all three boundary components are allowed to rotate. The flow can be expressed in terms of eddy functions in combination with forced modes induced by the driving. We have studied the complex power laws involved and determined the regions of parameter space where infinite sequences of eddies can occur. Using a collocation method we have constructed a number of example flows and visualized sequences of toroidal vortices near the apex. Depending upon the cone opening and the driving, eddies may also appear for symmetry reasons. We have also counted the number of visible eddies in the flow as a function of the driving parameters for examples of cone angles (α, β).

This work is currently being extended to non-axisymmetric Stokes flow: the flow is modelled in a similar fashion as in this paper with an azimuthal dependence in the form of complex exponential functions, just as in the single-cone case (**5**, **6**). The extension to a three-dimensional flow domain introduces a number of interesting questions regarding not only the existence of eddies but also their structure. Preliminary results suggest that, analogous to the flow in a single cone, the behaviour of the eigenvalue spectrum differs significantly with respect to the chosen azimuthal wave number.

Acknowledgements

We are grateful to Dr Richard Hewitt for useful discussions and for allowing us access to the unpublished notes (**13**). We also thank Professor Keith Moffatt who pointed out important references that were unknown to us, in particular (**15**), as well as Professor Andrew Soward for valuable comments on this work during its progression. The first author is grateful to the EPSRC for funding a Ph.D. studentship, under grant GR/T08968/01.

References

1. H. K. Moffatt, Viscous and resistive eddies near a sharp corner, *J. Fluid Mech.* **18** (1964) 1–18.
2. H. K. Moffatt and B. R. Duffy, Local similarity solutions and their limitations, *ibid.* **96** (1980) 299–313.
3. C. P. Hills, Eddies induced in cylindrical containers by a rotating end wall, *Phys. Fluids* **13** (2001) 2279–2286.
4. C. H. Liu and D. D. Joseph, Stokes flow in conical trenches, *SIAM J. Appl. Math.* **34** (1978) 286–296.
5. V. S. Malyuga, Viscous eddies in a circular cone, *J. Fluid Mech.* **522** (2005) 101–116.
6. P. N. Shankar, Moffatt eddies in the cone, *ibid.* **539** (2005) 113–135.
7. S. Wakiya, Axisymmetric flow of a viscous fluid near the vertex of a body, *ibid.* **78** (1976) 737–747.
8. N. Ohmura, M. N. Noui-Mehidi, K. Sasaki, K. Kitajima and K. Kataoka, Mixing characteristics in a conical Taylor–Couette flow system at low Reynolds numbers, *J. Chem. Eng. Japan* **37** (2004) 546–550.
9. O. A. Troshkin, Calculation of hydrodynamic characteristics of viscous fluid flow between rotating cones, *Teor. Osnovy Khim. Tekhnol.* **7** (1973) 897–903.
10. M. N. Noui-Mehidi, A. Salem, P. Legentilhomme and J. Legrand, Apex angle effects on the swirling flow between cones induced by means of a tangential inlet, *Int. J. Heat & Fluid Flow* **20** (1999) 405–413.
11. M. N. Noui-Mehidi, N. Ohmura and K. Kataoka, Dynamics of the helical flow between rotating conical cylinders, *J. Fluids Struct.* **20** (2005) 331–344.
12. M. Wimmer, Taylor vortex flow between conical cylinders, *J. Fluid Mech.* **292** (1995) 205–227.
13. R. E. Hewitt, Toroidal eddies in slowly swirling flows. Unpublished note (2005).
14. C. P. Malhotra, P. D. Weidman and A. M. J. Davis, Nested toroidal vortices between concentric cones, *J. Fluid Mech.* **522** (2005) 117–139.
15. T. P. Hynes, Stability of thin films, Ph.D. Thesis, University of Cambridge (1978).
16. G. I. Barenblatt, *Scaling, Self-Similarity and Intermediate Asymptotics*, Cambridge Texts in Applied Mathematics 14 (Cambridge University Press, Cambridge 1997).
17. H. K. Moffatt, The asymptotic behaviour of solutions of the Navier–Stokes equations near sharp corners, *Approximation Methods for Navier–Stokes Problems*, Lecture notes in Mathematics 771 (ed. R. Rautmann; Springer, Berlin 1979) 371–380.
18. C. P. Hills, Eddy structures induced within a wedge by a honing circular arc, *Theoret. Comput. Fluid Dynamics* **15** (2001) 1–10.
19. P. N. Shankar and M. D. Deshpande, Fluid mechanics in the driven cavity, *Ann. Rev. Fluid Mech.* **32** (2000) 93–136.
20. H. K. Moffatt and H. Kamkar, On the time-scale associated with flux expulsion, *Stellar and Planetary Magnetism* (ed. A. M. Soward; Gordon & Breach, New York 1983) 91–97.
21. P. B. Rhines and W. R. Young, How rapidly is a passive scalar mixed within closed streamlines? *J. Fluid Mech.* **133** (1983) 133–145.